Cellulose Acetate/Polysilsesquioxane Composites: Thermal Properties and Morphological Characterization by Electron Spectroscopy Imaging

Adair Rangel de Oliveira Junior, Márcia Maria Favaro Ferrarezi, Inez Valéria Pagotto Yoshida, Maria do Carmo Gonçalves

Institute of Chemistry, University of Campinas (UNICAMP), Campinas, SP, Brazil

Received 9 February 2011; accepted 17 April 2011
DOI 10.1002/app.34707
Published online 22 August 2011 in Wiley Online Library (wileyonlinelibrary.com).

ABSTRACT: Cellulose acetate (CA) composites using two types of silane coupling agents (methyltrimethoxysilane and phenyltriethoxysilane) were prepared through two methodologies: direct reaction between CA and the specific monomer and reaction of CA with oligomers, which were produced by prehydrolysis of the same monomers. The thermal behavior and morphology of the materials were studied. The composites showed thermal stability similar to pure CA, increase of residue content at 790°C and reduction in the glass transition temperature. Complementary microscopy techniques were applied to investigate the distribution of polysilsesquioxane in the CA matrix. Silicon mapping images showed the presence of domains with higher polysilsesquioxane concentration than the matrix and also the presence of silicon-rich nanodomains dispersed throughout the matrix. Based on mapping characterization, a schematic representation of the CA/polysilsesquioxane composite morphology was proposed. The organosilane type and architecture influenced the thermal behavior and the morphology of these materials. The results suggest that the silane coupling agents could be used to produce CA films with a range of properties. © 2011 Wiley Periodicals, Inc. J Appl Polym Sci 123: 2027–2035, 2012

Key words: cellulose acetate; composite; organosilane; morphology; silicon mapping

INTRODUCTION

Polymers from renewable resources have currently received considerable scientific, technical, and commercial interest mainly due to environmental issues, such as sustainability, the carbon cycle, biodegradation, and trends towards an understanding that petroleum resources are finite. An important class of biopolymers which can participate in the metabolic carbon cycle is cellulose esters. Cellulose acetate (CA) being the most commercially applied.[1–4]

CA is a thermoplastic produced primarily from cellulose. It has applications in many areas, such as, support for fibers, packing films, plastic devices, filters, membranes, adhesives, coating for papers, electrical isolation, and drug delivery systems.[3–6] However, several undesired characteristics including poor mechanical resistance, organic solvent attack, low swelling resistance in water, and low dimensional stability under high temperatures and humidity have limited the application of this polymer.[7,8] To overcome the limitations of CA and to expand, for example, its application in the field of membranes, some strategies have been applied, for instance: formation of polymer blends or composites, chemical modification and/or grafting.[7–23]

CA composites are reported in the literature, including composites prepared with inorganic particles, natural fibers, and also using silane coupling agents.[16,20–26] Introducing these fillers into CA offers the opportunity for the development of complex materials, which can improve thermal stability, mechanical resistance, and selective permeability of these materials.

The advantage of preparation of CA composites using silane coupling agents is the possibility to overcome some drawbacks, such as, limited filler addition content and filler agglomeration. In these systems, the dispersed inorganic phases can be obtained by hydrolysis followed by condensation reactions of alkoxysilane precursors, which can even be linked to the organic matrix.[27] The nature of the components and the composition of these films determine their characteristics.[20–23] Zoppi and Gonçalves[8] demonstrated that the incorporation of a silica phase, via sol–gel process by the hydrolysis of tetraethoxysilane, on a CA matrix led to more rigid films, which showed a decrease of water permeability, with thermal stability similar to pure CA.

Correspondence to: M. do C. Gonçalves (maria@iqm.unicamp.br).

Contract grant sponsors: FAPESP, CAPES.

Recently, Jiang and coworkers[28] developed CA membranes with enhanced permeation and antifouling properties. These materials were prepared through the *in situ* generation of silica nanoparticles, via the hydrolysis and condensation reaction of tetraethylorthosilicate as the precursor.

In a previous work,[29] CA/siloxane films were prepared using aminopropyltriethoxysilane, as a precursor. These films showed improved dimensional stability in comparison to pure CA. However, the influence of the silane architecture on the composite morphology was not explored. In this work, organic–inorganic composites derived from CA and two types of silane coupling agents were prepared. The preparation of CA/siloxane composites was carried out using two different approaches: direct reaction between CA chains and a monomer and reaction of CA with oligomers. Focus on the material morphology was given in this work, due to its direct relation with the material properties. Transmission electron microscopy analysis associated with electron loss spectroscopy (ESI-TEM) can give valuable and unambiguous information in elemental distribution. In this article, the morphology and the spatial distribution of silicon within the CA matrix were assessed by ESI-TEM.

EXPERIMENTAL

Materials

CA with a number-average molar mass of 30,000 g/mol, 39.8 wt % acetyl content (degree of CA substitution = 2.5) was purchased from Aldrich and was used as received. Methyltrimethoxysilane (MTMS) from Dow Corning, chemical formula $CH_3Si(OCH_3)_3$, and phenyltriethoxysilane (PhTES) from ABCR, chemical formula $C_6H_5Si(OC_2H_5)_3$, were used as silane coupling agents. Tetrahydrofuran (THF), purchased from Merck, was dried and distilled prior to use.

Preparation of the composites

Two preparation methods were evaluated: (A) direct use of the specific monomer as a modifier and (B) use of oligomers as modifiers, which were produced by prehydrolysis of the same monomers used in method A. 10 and 20 wt % silane coupling agent in relation to the amount of CA was added in both procedures.

Method (A): CA was dissolved in 50 mL THF in a flask connected to a reflux condenser. The solution was magnetically stirred and the monomer (MTMS or PhTES) was added to the flask in the desired proportion. A tin dibutyldiacetate solution (2 wt % in relation to the silane content) was used as catalyst, which promoted the self-condensation of the monomers. The reaction was carried out for 4 days under reflux at 60°C, under argon. The proposed mechanism is illustrated in Figure 1(a).

Method (B): In this method, the monomer (MTMS or PhTES) was prehydrolyzed in the presence of water prior to the reaction with CA. Prehydrolysis was conducted by adding water to the silane at a VTMS : H_2O molar ratio of 1 : 1, using also THF as a solvent and tin dibutyldiacetate as a catalyst. The mixture was then kept in a closed bottle and magnetically stirred for 15 min at room temperature. After the reaction, the solution was transferred to the flask containing CA solution in THF, in normal room environmental conditions. The proposed mechanism is illustrated in Figure 1(b).

The viscous homogeneous solutions obtained from methods A and B were cast onto Teflon™ Petri dishes and left to dry in a vacuum oven at 50°C for 2 days. Table I indicates the composition of the samples prepared and the name (code) assigned for each one.

Characterization

Infrared spectra were performed on a Bomem MB B100 Series spectrometer operating at a 4 cm^{-1} resolution and coadding 16 scans in the region between 400 and 4000 cm^{-1}, with the conventional KBr-supported film technique. Thermogravimetric analysis (TGA) was performed in a TA 2950 thermobalance, TA Instruments, in the 30–950°C range, at a 20°C/min scanning rate under an argon flow. Differential scanning calorimetry analyses (DSC) were conducted on a DSC model 2910, TA Instruments, operating under an argon atmosphere. The thermal curves were obtained from dried samples and by the following procedure: heating from 30 to 280°C at 20°C/min; isotherm for 5 min; cooling to −50°C at 20°C/min; isotherm for 15 min; heating to 280°C at 20°C/min.

The morphology of the samples was examined with a JSM-6340 field emission scanning electron microscope (FESEM) from Jeol Ltd., operating at an accelerating voltage of 3.0 kV. The samples were prepared by fracturing in liquid nitrogen followed by carbon and gold sputtered coating in a Bal-Tec MD 020 instrument (Balzers). The morphology of the samples was also investigated in a Carl Zeiss CEM902 transmission electron microscope associated with electron loss spectroscopy (ESI-TEM). The microscope was operated at an acceleration voltage of 80 kV and equipped with a Castaing-Henry energy filter spectrometer within the column. Ultrathin sections, approximately 40 nm thick, were cut at room temperature (~ 26°C) using a diamond knife, in a Leica EM FC6 cryo-ultramicrotome.

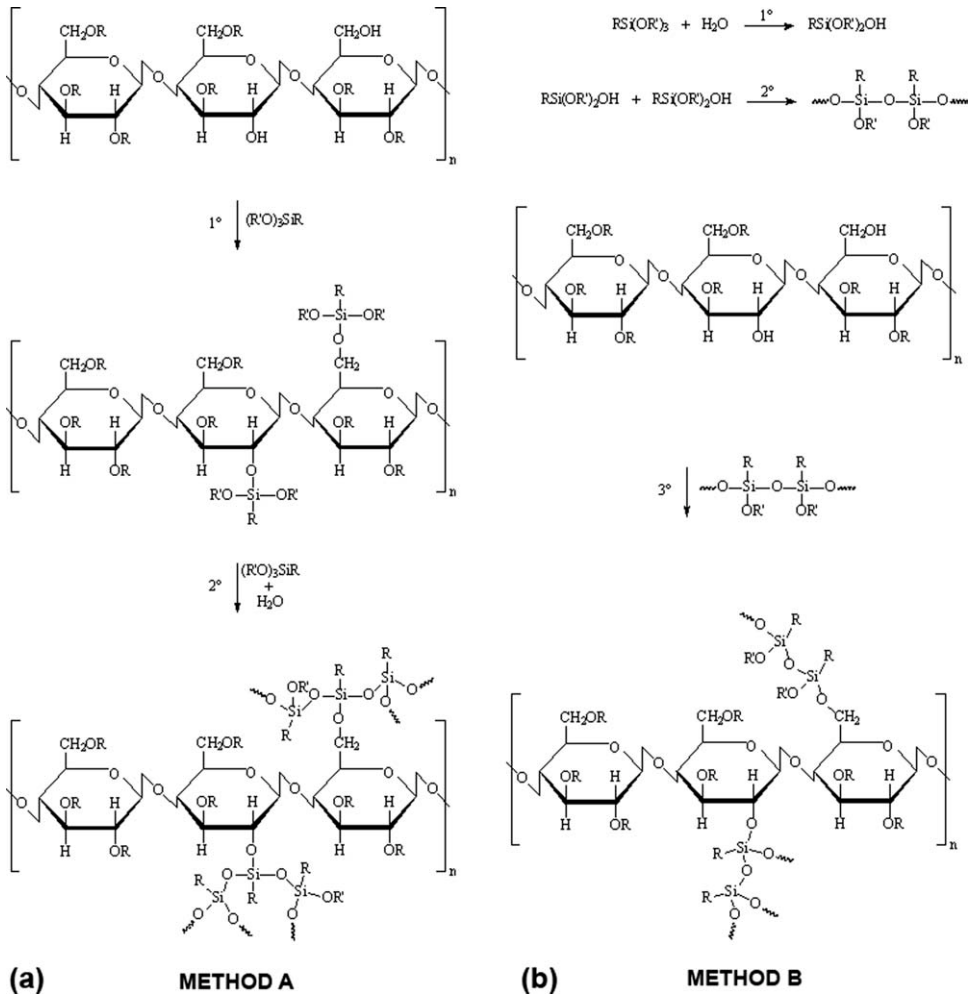

Figure 1 Proposed mechanisms for CA modification: (a) method A and (b) method B.

Elemental images were obtained for silicon, the characteristic element in the modifiers, using an energy-selecting slit of 15 eV and the three-window method. The energy-selecting slit was set at 132 eV for Si, which corresponds to the silicon $L_{2,3}$-edge. To make sure that sample thickness was adequate for elemental mapping, the image contrast inversion was monitored, as the energy loss of the electrons used for energy-filtered imaging was changed from 0 to 20 eV. The images were recorded using a Proscan high-speed slow-scan CCD camera and processed using the AnalySis software.

RESULTS AND DISCUSSION

The CA/MTMS sample resulted in slightly opaque films. On the other hand, films of CA/PhTES were transparent (except for the CA/20PhTES sample), which indicates that phase separation did not occur with these samples or that if a dispersed polysiloxane phase had developed in the CA matrix, this phase was on a submicron scale. Similar behavior was observed in a previous work,[29] where the prepared siloxane-modified CA films were characterized by siloxane nanodomains dispersed in the CA matrix, with good interfacial adhesion between the phases. The nanodomains were smaller than the wavelength of visible light so that the materials were optically clear.

The infrared spectra are shown in Figure 2. For pure CA, a characteristic carbonyl (C=O) stretching band around 1754 cm^{-1} and a characteristic

TABLE I
Composition of the CA Composites

Sample name	Reaction method	Modifier	Silane content (wt %)
CA/10MTMS	A	MTMS	10
CA/10MTMS-pr	B	MTMS	10
CA/20MTMS	A	MTMS	20
CA/20MTMS-pr	B	MTMS	20
CA/10PhTES	A	PhTES	10
CA/10PhTES-pr	B	PhTES	10
CA/20PhTES	A	PhTES	20
CA/20PhTES-pr	B	PhTES	20

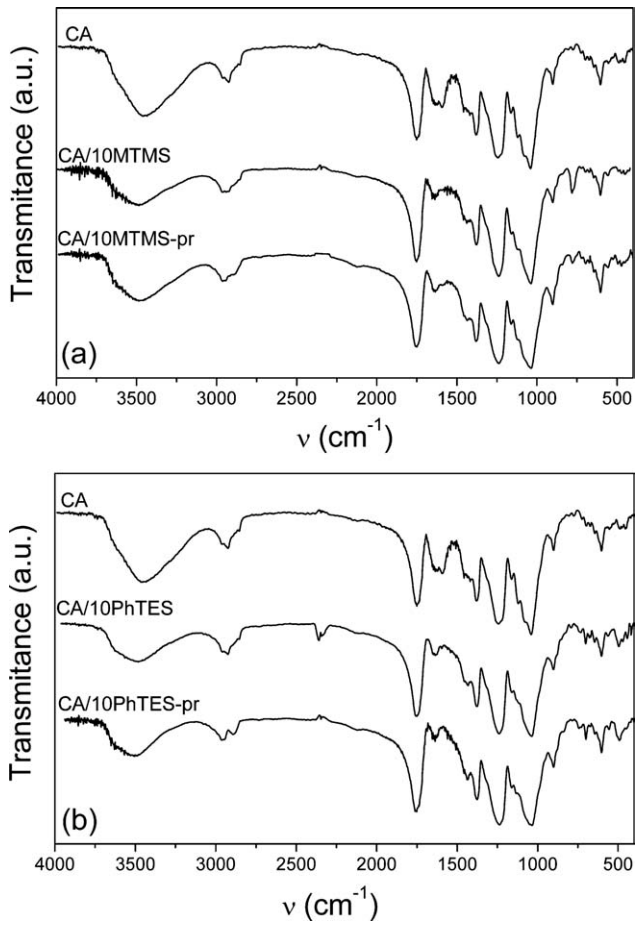

Figure 2 FTIR spectra: (a) pure CA and CA composites generated from MTMS and (b) pure CA and CA composites generated from PhTES.

hydroxyl (O—H) stretching band at 3460 cm^{-1} were observed. The spectra of the CA/MTMS composites [Fig. 2(a)] show an absorption band around 781 cm^{-1}, assigned to Si—C stretching of the $Si—CH_3$ group from MTMS. For both CA composite spectra a reduction in the intensity of the band at $\sim$ 3460 cm^{-1} was also observed, which is an indication of the reduction of OH group content due to the reaction between the CA chains and the organosilane. The same behavior was observed for the CA/PhTES samples, as shown in Figure 2(b).

The thermogravimetry curves for pure CA and composites are shown in Figure 3. In the case of CA, three steps of mass loss were observed. The first step from 32 to 180°C represents the volatilization of residual water and the second step, from 180 to 300°C, is related to the loss of acetyl groups, followed by acetic acid volatilization, which could catalyze the decomposition of cellulose. The third step starts at 300°C and represents the main thermal degradation of cellulose chains. This degradation profile is in agreement with the Chatterjee and Conrad's[30] description for cellulosic materials.

For the CA composites, there is an initial mass loss between 175 and 210°C which could be a consequence of the organosilane condensation reactions which eliminate water, methanol, or ethanol. In all materials, the maximum degradation rate was between 350 and 400°C.

Moreover, after 790°C, the pure CA presented practically no residue. However, a considerable residue amount for the samples of CA composites was observed, probably consisting of SiCxOy,[31,32] which is the pyrolysis product, under an inert atmosphere, of the polysilsesquioxane component formed by the polycondensation of the silane grafted into the CA chains. Table II shows the residue amount of each sample. All CA composites presented this thermal behavior, suggesting that the incorporation of the polysiloxane phase into the CA was obtained in all samples. When the residue amount is compared, the preparation carried out by the method B resulted in a larger residue percentage, which can be related to

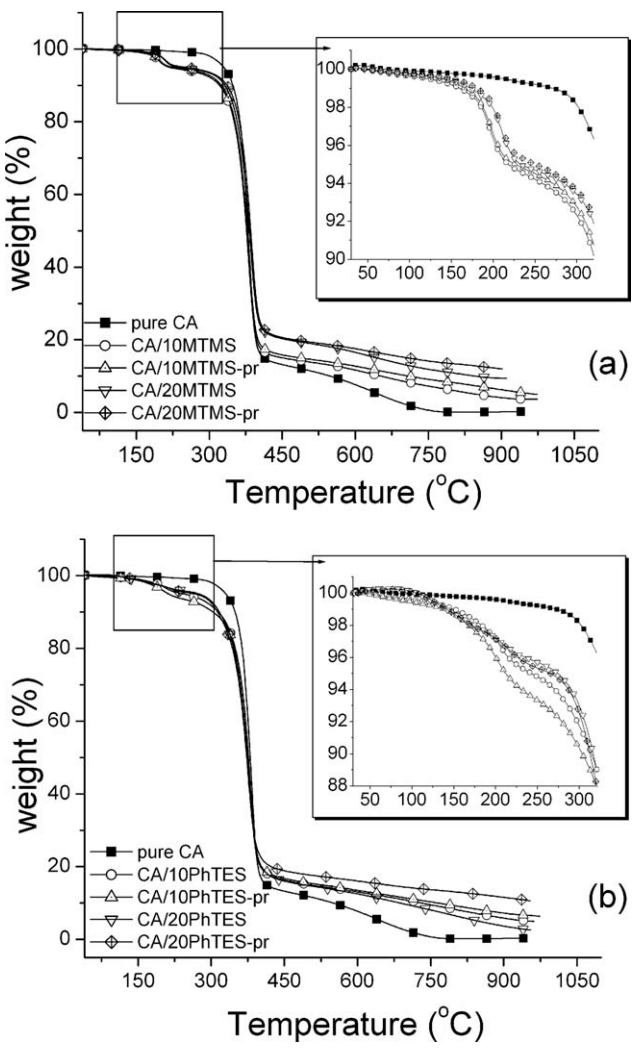

Figure 3 Thermogravimetric curves of pure CA and CA composites: (a) MTMS and (b) PhTES.

TABLE II
TG and DSC Results for CA and CA Composites

Sample name	Residue (%)	T_g (°C)	T_M (°C)
Pure CA	0.15	161	197
CA/10MTMS	6.30	143	–
CA/10MTMS-pr	8.41	124	–
CA/20MTMS	11.07	122	–
CA/20MTMS-pr	13.54	102	–
CA/10PhTES	8.36	161	–
CA/10PhTES-pr	9.35	137	–
CA/20PhTES	6.69	173	–
CA/20PhTES-pr	13.11	149	–

a higher incorporation of silane by this procedure. However, no influence of the methodology on the initial mass loss was observed. Stiubianu et al.[7] also observed an increase of the residue amount with the addition of siloxane in CA.

Table II also illustrates the thermal behavior of the samples obtained by DSC. For pure CA, the measured glass transition temperature (T_g) was 161°C and the melting temperature (T_M) was 197°C. In the CA composite obtained using MTMS by method A, a shift to lower T_g values was observed. This decrease was enhanced by the increase of the MTMS content (CA/10MTMS and CA/20MTMS samples) and, furthermore, no melting transition was observed. For the composites prepared by method B (prehydrolysis of the monomers) the T_g values were even lower. Glasser et al.[33] also observed a reduced in T_g value and the disappearance of melting transition with the increase in length of a fluoralkoxy chain grafted onto the CA chains.

In the case of CA/PhTES samples, no melting transition was observed and also a decrease in the T_g values was obtained but only for the CA/10PhTES-pr and CA/20PhTES-pr samples (method B).

These different behaviors for the CA composites could be interpreted by the contribution of three factors: (i) increase in free volume due to the insertion of polymer side groups,[34] (ii) high flexibility of the side group, due to the presence of Si—O—Si groups,[35] and (iii) reduction of hydrogen bonds due to the substitution of the hydroxyl groups by organosilanes, which contributes as an extra factor to the increased mobility of the modified polymer.

The free volume effect is better analyzed comparing the results from the composites with the same organosilane content. It is observed that the organosilane insertion under the oligomer form (method B) causes a more pronounced effect on T_g reduction of the CA chains. This effect can be related to the higher free volumes of these oligomeric groups than that of the corresponding grafted monomers. The possibility of some extent of grafting of organosilanes on the CA chains interferes with the structural regularity of this polymer, and consequently in the crystallization behavior of CA chains. For CA/10PhTES and CA/20PhTES samples, a decrease in the T_g values was not observed. This behavior could be attributed to the stiffening imposed by the phenyl groups. The literature indicates that the insertion of these side groups usually increases main-chain stiffness, an effect ascribed to interaction (steric hindrance) between the side groups.[36] Thus, in this study, the presence of large and bulky side groups tend to cause stiffening which seems to be predominant over the effect of the free volume increase caused by the insertion of organosilane side groups into CA chains.

Figure 4 presents the morphology of pure CA bulk fracture investigated by FESEM. The fractured surface morphology is relatively rough, showing cavities generated during the fracture of the sample.

The micrographs in Figure 5 refer to the CA/20MTMS and CA/20MTMS-pr samples. Typical composite morphology is observed for both samples due to the presence of spherical domains in the matrix, confirming the formation of CA/polysilsesquioxane composites. The average diameter of these domains was 3.0 ± 1 μm for the CA/20MTMS and CA/20MTMS-pr composites. The cavities are due to particles that were detached from the matrix after the fracture, showing that there is low adhesion between the phases, due to the apolar characteristics of the methyl group of the poly(methylsilsesquioxane) domains. Poly(methylsilsesquioxane)s generated from MTMS condensation present low solubility in many organic solvents.[37] This low solubility may be the main factor responsible for the phase separation of the components, while still in solution.

The micrographs of CA composites obtained using PhTES are shown in Figure 6. In these surface fractures, no phase separation was detected by this microscopic technique. The apparent change of phase

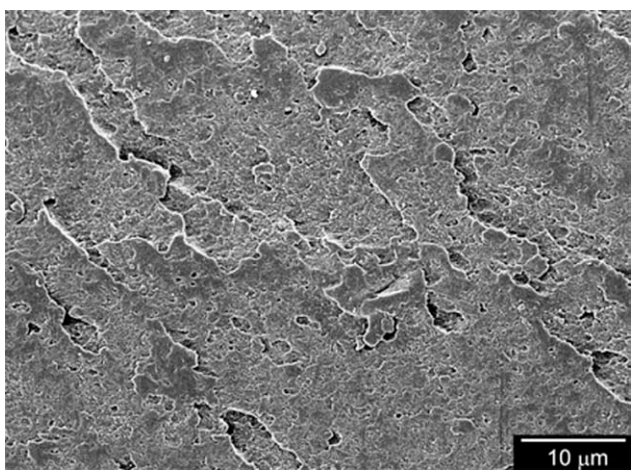

Figure 4 FESEM micrograph of bulk fracture of pure CA.

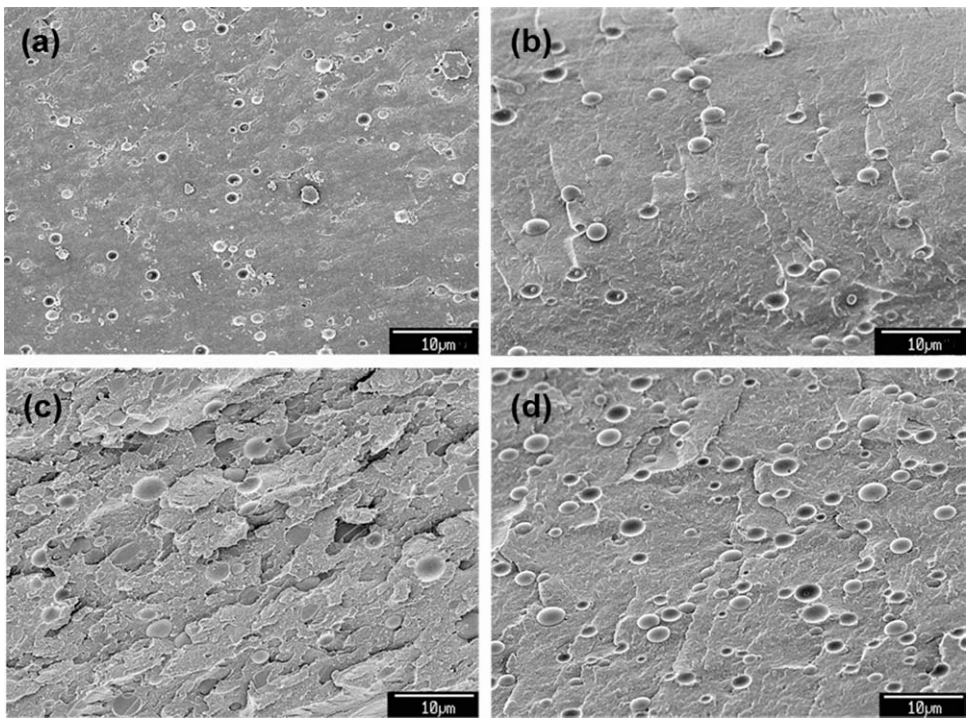

Figure 5 FESEM micrographs of bulk fractures: (a) CA/10MTMS, (b) CA/10MTMS-pr, (c) CA/20MTMS, and (d) CA/20MTMS-pr.

behavior in CA samples modified with PhTES can be justified by the high affinity of CA for chemical compounds containing electron-rich pendant groups,[38] such as the phenyl groups in this case. Moreover, the high solubility of the PhTES condensation products in THF is another aspect to be considered as being responsible for the morphology developed by these materials.[37]

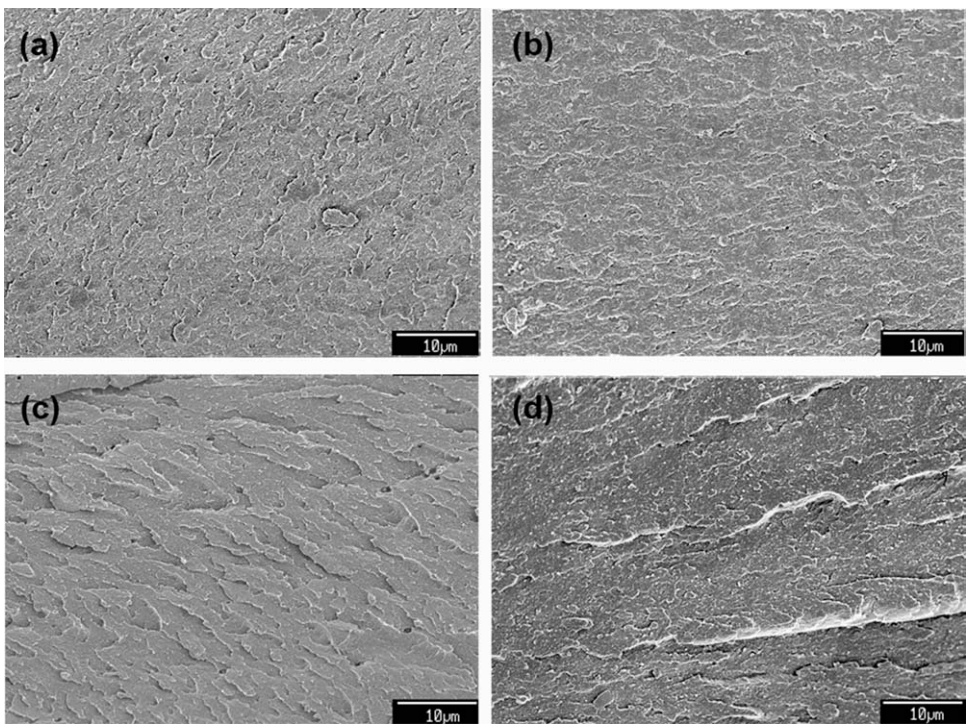

Figure 6 FESEM micrographs of bulk fractures: (a) CA/10PhTES, (b) CA/10PhTES-pr, (c) CA/20PhTES, and (d) CA/20PhTES-pr.

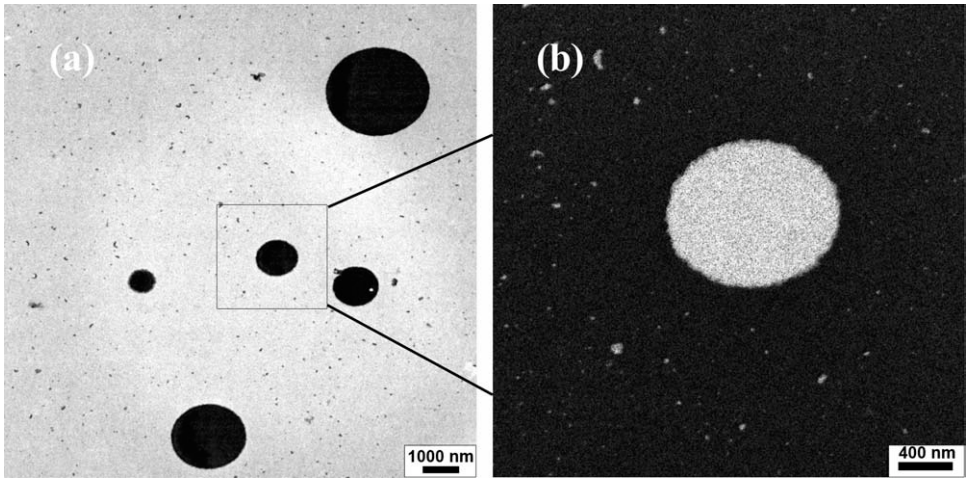

Figure 7 ESI-TEM images of the CA/20MTMS composite: (a) bright field and (b) silicon map.

Transmission electron microscopy analyses were employed to better assess the morphology of the composites obtained from the CA modification with methyltrimethoxysilane, as well as to evaluate the apparent change of phase behavior in CA composites generated from phenyltriethoxysilane. While conventional transmission electron microscopy uses elastically scattered electrons for generation of the

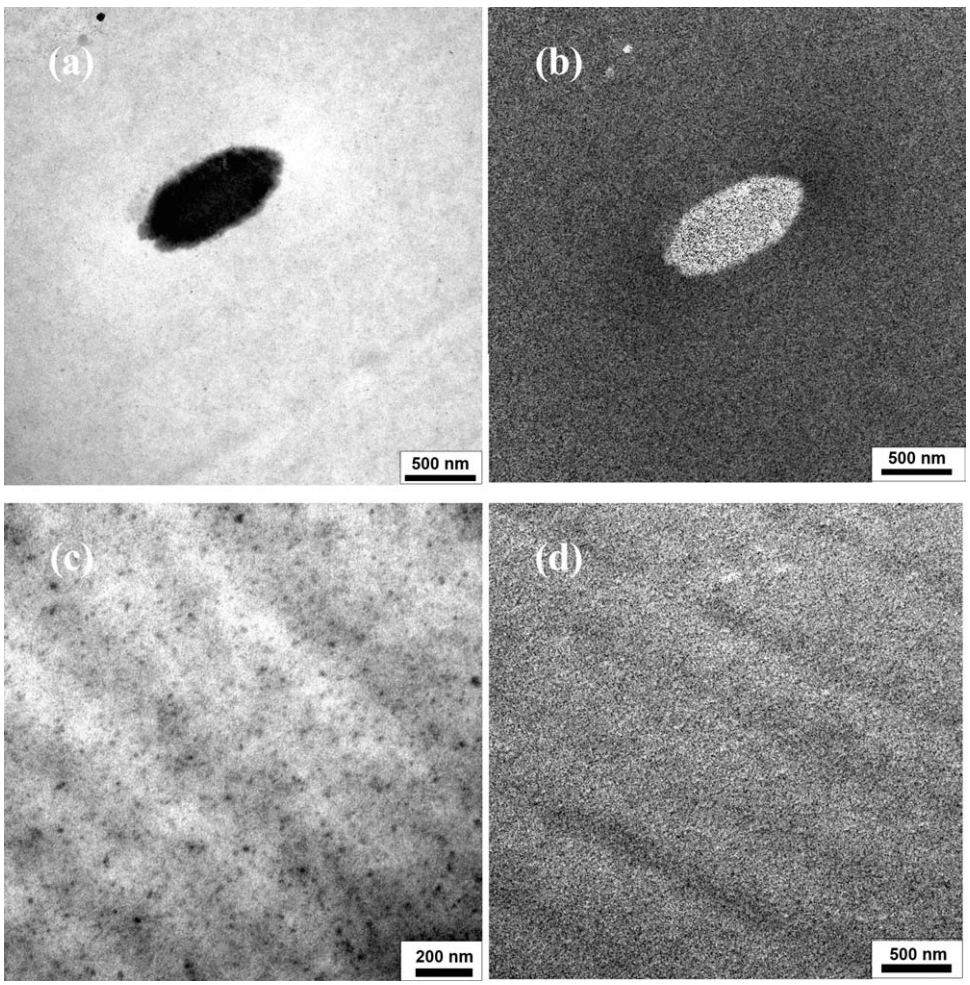

Figure 8 ESI-TEM images: (a) CA/20PhTES bright field, (b) CA/20PhTES silicon map, (c) CA/20PhTES-pr bright field, and (d) CA/20PhTES-pr silicon map.

micrograph image, element spectroscopic imaging uses the inelastically scattered ones. Electrons passing through the specimen undergo a specific energy loss, which depends on the elements present at the location of transit. The electrons are separated with respect to their energies and images are generated using these "mono-energetic" electrons, thus showing the net element distribution in the samples.[39] The compositional morphology of CA composites was confirmed by ESI-TEM, mapping the silicon distribution to obtain polysilsesquioxane distribution across the CA matrix.

The bright field and the silicon mapping images of the CA/20MTMS composite are shown in Figure 7(a,b), respectively. In the bright field image [Fig. 7(a)], the dark regions are related to the denser phase, i.e., the polysilsesquioxane phase, and correspond to the white regions in the silicon mapping [Fig. 7(b)]. The silicon map shows the presence of this element in the entire image but more concentrated in some regions. The presence of scattered regions with higher density than the matrix is observed in the bright field image [Fig. 7(a)], showing domains with average diameter of 1.7 ± 0.8 μm. The silicon mapping image [Fig. 7(b)] shows that these domains present higher polysilsesquioxane concentration than the matrix and that silicon-rich nanodomains are also dispersed throughout the matrix.

Bright field images of the modified samples with 20 wt % of PhTES are shown in Figure 8(a,c). Areas consisting of polysilsesquioxane domains, which were not detected by the scanning electron microscopy analyses, can now be observed. Domains with 20 ± 10 nm average diameter of the CA/20PhTES-pr composite were smaller than the domains of the CA/20PhTES composite (average diameter of 1 μm). However, a lower concentration of such microdomains was observed when compared to the microdomain concentration presented in CA composite obtained using MTMS. The silicon mapping images are illustrated in Figure 8(b,d) for the CA samples modified with 20 wt % of PhTES. The poly(phenylsilsesquioxane) was distributed in the domains and also in the matrix for both samples. This distribution is more uniform in the CA/20PhTES-pr composite, showing again that the CA composite generated from oligomers enhances system homogeneity. In addition, the presented graft polymer could act as a compatibilizer between the condensation products and the matrix, improving phase dispersion.

The TEM images have complemented the FESEM analysis, allowing the identification of rich polysilsesquioxane areas. Therefore, it can be pointed out that the silane type and architecture were influential in the morphology developed by the CA composites.

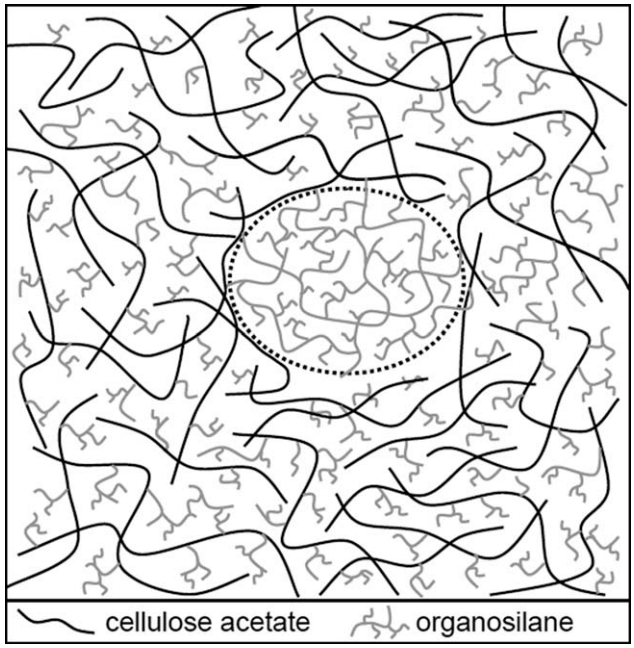

Figure 9 Synthetic concept of cellulose acetate/polysilsesquioxane composite.

Based on TEM observations, a schematic representation of the CA/polysilsesquioxane composites morphology is proposed, as can be seen from Figure 9. This representation is coherent with the result that the organosilanes were incorporated in the matrix, but preferentially located in dispersed micro and nanodomains formed by polysilsesquioxane.

CONCLUSIONS

The preparation of CA composites, using silane coupling agents by two different methodologies, was described. The CA/polysilsesquioxane composites showed thermal stability similar to pure CA, but the residue content at 790°C increased with silane addition. Reduction in the glass transition temperatures and disappearance of melting transition were also observed in the composites. Bright field and silicon mapping images showed that the dispersed domains present higher polysilsesquioxane concentration than the matrix and that silicon-rich nanodomains are also dispersed in the matrix. A more uniform morphology, with nanosized dispersed phases, was obtained for the composites prepared from phenyltriethoxysilane by method B. Based on mapping characterization, a schematic representation of the CA/polysilsesquioxane composite morphology was proposed. It was concluded that the organosilane type and the methodology applied for preparation of CA composites influenced the thermal behavior and morphology of the materials. Further studies on the composite permeability will focus on these

materials, expecting that CA/PhTES-pr films show a combination of appropriate permeability rate and selectivity for gases.

References

1. Williams, C. K.; Hillmyer, M. A. Polym Rev 2008, 48, 1.
2. Chandra, R.; Rustgi, R. Prog Polym Sci 1998, 23, 1273.
3. Edgar, K. J.; Buchanan, C. M.; Debenhan, J. S.; Rundquist, P. A.; Seiler, B. D.; Shelton, M. C.; Tindall, D. Prog Polym Sci 2001, 26, 1605.
4. Balser, K.; Eicher, T.; Wnadel, M.; Astheinmer, H. J. In Cellulose Esters. Ulmann's Encyclopedia of Industrial Chemistry; Gerhartz, W.; Yamamoto, Y. S., Eds.; VCH: Weinheim 1986, Vol.A5, 438.
5. Basu, S.; Khan, A. L.; Cano-Odena, A.; Liu, C.; Vankelecom, I. F. J Chem Soc Rev 2010, 39, 750.
6. Fischer, S.; Thümmler, K.; Volkert, B.; Hettrich, K.; Schmidt, I.; Fischer, K. Macromol Symp 2008, 262, 89.
7. Stiubianu, G.; Racles, C.; Cazacu, M.; Simionescu, B. C. J Mater Sci 2010, 45, 4141.
8. Zoppi, R. A.; Gonçalves, M. C. J Appl Polym Sci 2002, 84, 2196.
9. Saljoughi, E.; Mohammadi, T. Desalination 2009, 249, 850.
10. Gulec, H. A.; Topacli, A.; Topacli, C.; Albayrak, N.; Mutlu, M. J Membr Sci 2010, 350, 310.
11. Sikder, J.; Pereira, C.; Palchoudhury, S.; Vohra, K.; Basumatary, D.; Pal, P. Desalination 2009, 249, 802.
12. Cerqueira, D. A.; Valente, A. J. M.; Filho, G. R.; Burrows, H. D. Carbohydr Polym 2009, 78, 402.
13. Boricha, A. G.; Murthy, Z. V. P. Chem Eng J 2010, 157, 393.
14. Onish, M.; Takahashi, S.; Namikoshi, H.; Asami, M. Jpn Pat.60,188,401 (1995).
15. Ohga, A.; Namikoshi, H. G. B. Daicel Chem Ind Ltd., Pat.2,152,944 (1985).
16. Wara, N. M.; Francis, L. F.; Velamakanni, B. V. J Membr Sci 1995, 104, 43.
17. Nie, L.; Narayan, R. J Appl Polym Sci 1994, 54, 601.
18. Chen, W.; Su, Y.; Zheng, L.; Wang, L.; Jiang, Z. J Membr Sci 2009, 337, 98.
19. Billy, M.; Costa, A. R.; Lochon, P.; Clément, R.; Dresch, M.; Jonquières, A. J Membr Sci 2010, 348, 389.
20. Bandyopadhyay, A.; Bhowmick, A. R.; De Sarkar, M. J Appl Polym Sci 2004, 93, 2579.
21. Amerio, E.; Sangermano, M.; Malucelli, G.; Priola, A.; Voit, B. Polymer 2005, 46, 11241.
22. Mark, J. E.; Lee, C.; Bianconi, P. A. Hybrid Organic–Inorganic Composites; ACS: Washington, 1995; Vol.585.
23. Mackenzie, J. D.; Bescher, E. J Sol–Gel Sci Tech 2003, 27, 7.
24. Arthanareeswaran, G.; Thanikaivelan, P. Sep Purif Technol 2010, 74, 230.
25. Tsioptsias, C.; Sakellariou, K. G.; Tsivintzelis, I.; Papadopoulou L.; Panayiotou, C. Carbohydr Polym 2010, 81, 925.
26. Lu, J.; Drzal, L. T. J Polym Sci Part B Polym Phys 2010, 48, 153.
27. Britcher, L. G.; Kehoe, D. C.; Matisons, J. G.; Swincer, A. G. Macromolecules 1995, 28, 3110.
28. Chen, W.; Su, Y.; Zhang, L.; Shi, Q.; Peng, J.; Jiang, Z. J Membr Sci 2010, 348, 75.
29. Silva, C.A.; Favaro, M. M.; Yoshida, I. V. P.; Gonçalves, M. C. J Appl Polym Sci 2011, 121, 2559.
30. Chatterjee, P. K.; Conrad, C. M. J Polym Sci Part A Polym Chem 1968, 6, 3217.
31. Schiavon, M. A.; Redondo, S. U. A.; Pina, S. R. O.; Yoshida, I. V. P. J Non-Cryst Sol 2002, 304, 92.
32. Radovanovic, E.; Gozzi, M. F.; Gonçalves, M. C.; Yoshida, I. V. P. J Non-Cryst Sol 1999, 248, 37.
33. Glasser, W. G.; Becker, U.; Todd, J. G. Carbohydr Polym 2000, 42, 393.
34. Seymour, R. B. Structure–Property Relationships in Polymers; Plenum Press: New York, 1989.
35. Hardman, B.; Torkelson, A. In Silicones. Encyclopedia of Polymer Science and Technology; Mark, H. F.; Bikales, N. M.; Overberger, C. G.; Menges, G., Eds.; Wiley: New York, 1996; Vol.15, 204.
36. Tsvetkov, V. N.; Eskin, V. E.; Frenkel, S. Y. Structure of Macromolecules in Solutions; Nat Lending Lib Sci Tech: Boston, 1971.
37. Ronald, H. B. Chem Rev 1995, 95, 1409.
38. Kim, B. K.; Oh, Y. S.; Lee, Y. M.; Yoon, L. K.; Lee, S. Polymer 2000, 41, 385.
39. Ribbe, A.; Prucker, O.; Rühe, J. Polymer 1996, 37, 1087.